VNU Journal of Science: Mathematics - Physics

Journal homepage: https://js.vnu.edu.vn/MaP

Original Article

Study on Gas Adsorption Properties (N_2, H_2, O_2, NO, NO_2, CO, CO_2, SO_2, H_2S, H_2O and NH_3) on the O-vacancy-containing Sc_2CO_2 Monolayer

Pham Dinh Khang[1,*], Luong Le Hai[2], Nguyen Thi Tham Hong[3], Vu Van Tuan[3],

[1]*Military Institute of Mechanical Engineering, 42 Dong Quan, Nghia Do, Cau Giay, Hanoi, Vietnam*

[2]*Ho Chi Minh City University of Education, 280 An Duong Vuong, District 5, Ho Chi Minh City, Vietnam*

[3]*Institute for Computational Science, Ton Duc Thang University,*

19 Nguyen Huu Tho, Tan Phong, District 7, Ho Chi Minh City, Vietnam

Received 9 June 2021
Revised 12 July 2021; Accepted 29 July 2021

Abstract: In this work, we have studied the (N_2, H_2, O_2, NO, NO_2, CO, CO_2, SO_2, H_2S, H_2O, and NH_3) gases adsorption properties on the O-vacancy-containing Sc_2CO_2 monolayer by first-principles calculations. We have determined the preferred adsorption positions and the structural features of the O-vacancy-containing Sc_2CO_2 monolayer after adsorption of different gas molecules. The adsorption energy and charge transfer from the monolayer to the gas molecules have been calculated. The calculated results show that H_2, N_2, NH_3, H_2S and H_2O molecules are physisorbed, while CO_2, CO, NO_2, NO, O_2 and SO_2 molecules are chemisorbed in the neighboring area of the O-vacancy of the Sc_2CO_2 monolayer. The existence of the O-vacancy significantly enhances the CO and CO_2 adsorption intensity of the defect Sc_2CO_2 monolayer compared to the original Sc_2CO_2 monolayer. Our results show that the O-vacancy-containing Sc_2CO_2 monolayer can be used for detecting NO gas as a resistive sensor.

Keywords: gas adsorption, Sc_2CO_2 monolayer, vacancy defect, first-principles calculations.

1. Introduction

Gas sensors and gas capture devices are widely applied in human life, medical, military, and industry to detect and capture various gases [1]. The selectivity, response time, reusability of gas

* Corresponding author.
E-mail address: dinhkhang307@gmail.com

https//doi.org/10.25073/2588-1124/vnumap.4653

sensors and gas storage capacity of capture devices can be improved by applying two-dimensional materials with superior surface area to volume ratios than bulk materials [2-4].

The MXenes-type two-dimensional (2D) material was discovered in 2011 [5] with a structure of the form of $M_{n+1}X_n$, where "M" is a transition metal (Sc, Ti, Zr, Hf, V, Nb, Ta, Cr or Mo), "X" is carbon or nitro and n = 1, 2 or 3. Recently, several other MXenes materials have been discovered including M_2B, M_2B_2 and M_3B_4, where 'M' is Ti, Zr or Hf element; B is Boron element [6, 7]. 2D MXenes are reported as potential materials in the field of gas sensing and gas capture due to their high surface-to-volume ratio and excellent electronic properties [5, 8-11]. The gas adsorption properties on the surface are the basis for determining the applications of the materials in the aforementioned fields. In recent years, the gas adsorption properties on 2D Mxenes materials have attracted great research. The MXenes Ti_2CO_2 monolayer selectively adsorbs NH_3 molecules over H_2, CO_2, O_2, N_2, NO_2, CH_4 and CO gas molecules and has a large sensitivity to NH_3 compared to MoS_2 and phosphorene [12], which gives potential application of 2D Ti_2CO_2 materials in gas sensors or NH_3 gas storage devices with large selectivity and sensitivity. In addition, Ti_3C_2 MXenes can be used to CO_2 capture and conversion in low pressure with high capacities up to ≈12 mol/kg because of its high adsorption efficiency, selectivity of CO_2 adsorption compared to N_2 and its chemical and thermal stability [13, 14]. In addition, Ti3C2 Mxenes can be applied for sensing ethanol, methanol, acetone and ammonia gases at room temperature. Junkaew et al. [15] demonstrated that surface termination with oxygen atoms of MXenes of the form M_2C (M = Ti, V, Nb or Mo) reduces the adsorption capacity, but improves the adsorption selectivity. Accordingly, Mo_2CO_2 and V_2CO_2 have good selectivity for NO molecules, while Nb_2CO_2 and Ti_2CO_2 reveal large selectivity for NH_3 adsorption.

The Sc_2C monolayer possesses the highest surface area per weight compared to other materials of the MXenes family [16]. It is known that the 2D Sc_2CO_2 has the highest hydrogen storage capacity due to the Kubas-type effect [17, 18]. The applicability of the Sc_2CO_2 monolayer gas sensors has been considered by studying adsorption intensity, selectivity and conductivity change effect when adsorbing gas such as NO gas sensor [19] or SO2 gas sensor [20]. The CO adsorption on the Sc_2CO_2 monolayer is significantly improved by Mn atomic doping [19]. Recently, Pham et al. [21] reported that NO, O_2, SO_2 and NO_2 gases were chemisorbed on the original Sc_2CO_2 monolayer, where the adsorption selectivity for oxygen molecule limits its applicability in gas sensor or gas capture. This leads to the need to consider tuning the gas adsorption properties of the Sc_2CO_2 monolayer by vacancies, which can be generated by the electron beam [22] and significantly alter the electronic and transport properties of 2D structures [22-24].

Therefore, we have studied the gas adsorption properties, including harmful gases (NO, NO_2, CO, SO_2, H_2S and NH_3) and components in clean air (N_2, H_2, O_2, CO_2 and H_2O) on the O-vacancy-containing Sc_2CO_2 monolayer. The preferred adsorption sites, the structural features, adsorption distance, adsorption energy, charge transfer have been determined. In this work we have also elucidated the selectivity of the gas adsorption on the O-vacancy-containing Sc_2CO_2 monolayer.

2. Computational Details

In this work, all of the first-principles calculations were performed using Quantum Espresso software package [25] within Perdew–Burke–Ernzerhof generalized gradient approximation (PBE-GGA) [26, 27]. We use Grimme's semiempirical DFT-D2 method to account for Van der Waals (vdW) interactions between atoms in the structural model [28]. The Sc_2CO_2 supercell which used in the calculations was constructed by stacking 3×3×1 unit cell (Figure 1b). The thickness of the vacuum

layer was set to 15 Å to avoid interactions between the monolayers. Optimization calculations for the Sc_2CO_2 monolayer structure were performed to determine its optimized cell parameters.

The grid of k-points is set to 6x6x1 according to the Monkhorst-Pack scheme. Kinetic energy cutoff for wavefunctions and for charge density were set as 30 Ry and 300 Ry, respectively. Optimized calculations are performed until the total forces in the supercell are less than 0.01 eV/Å. The convergence threshold for selfconsistency is set to 10^{-6} Ry. We investigated the interaction of gas molecules with the O-vacancy-containing Sc_2CO_2 monolayer from three possible initial adsorption sites: "A" site denotes the upper position of the O-vacancy, "B" and "C" sites denote the upper position of Sc atom at the second and fourth atomic layers, respectively (Figure 1 (d)). At the initial position, the N_2, H_2, O_2, NO, NO_2, CO, CO_2, SO_2, H_2S, H_2O and NH_3 gas molecules were located to be parallel to the Sc_2CO_2 monolayer and at a distance of 3.0 Å.

To understand the nature of the interaction between gas molecules and the O-vacancy containing Sc_2CO_2 monolayer, the density of state (DOS) of the system after gas adsorption was calculated and analyzed. The adsorption energy of gas molecules on the O-vacancy-containing Sc_2CO_2 monolayer is determined by formula [29]:

$$E_{ads} = E_{Sc_2CO_2{}^{Ov}} + E_{gas} - E_{gas+Sc_2CO_2{}^{Ov}}$$

where $E_{Sc_2CO_2{}^{Ov}}$ and $E_{gas+Sc_2CO_2{}^{Ov}}$ are the total energy of the O-vacancy-containing Sc_2CO_2 monolayer before and after gas molecule adsorption, respectively; E_{gas} is the total energy of the free gas molecules. All the aforementioned total energies are calculated with the same size of the supercells.

The charge transfers from the Sc_2CO_2 monolayer to the gas molecules are calculated by the change of the total charge of the gas molecules before and after being adsorbed on the monolayer. To calculate the total charge of each atom in the studied models, we used Bader population analysis [30, 31].

3. Results and Discussion

3.1. Geometric Structure of the O-vacancy-containing Sc_2CO_2 Monolayer

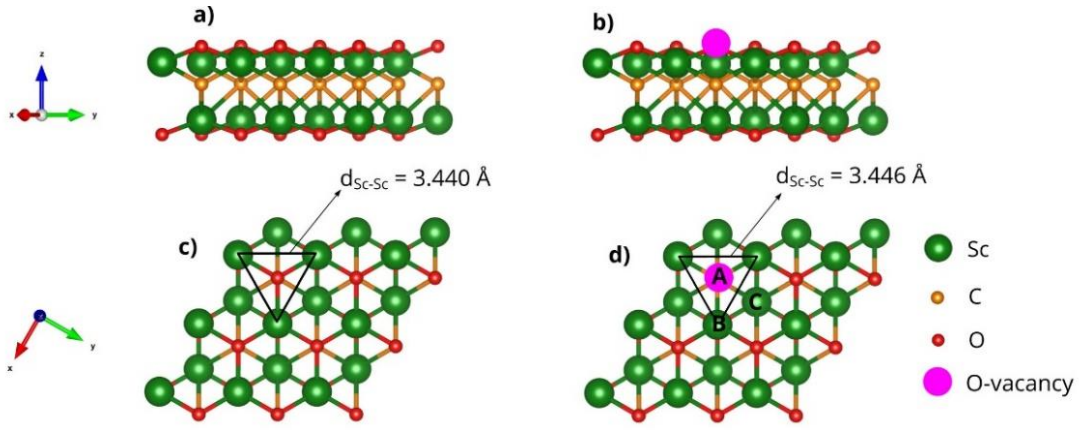

Figure 1. Side view and top view of the optimized structure of the ideal Sc_2CO_2 monolayer (a, c) and the O-vacancy-containing Sc_2CO_2 monolayer (b, d).

The optimized structure of the O-vacancy-containing Sc_2CO_2 monolayer is shown in Figure 1(b). When an oxygen vacancy occurs on the Sc_2CO_2 monolayer, the Sc atoms neighboring the oxygen vacancy move slightly away from the vacancy (Figure 1(a, b)). The distance between two adjacent Sc atoms on the ideal Sc_2CO_2 monolayer is 3.440 Å, while this value near the vacancy increases by 3.446 Å.

3.2. Physical Adsorption of H_2, N_2, NH_3, H_2S and H_2O Molecules on the O-vacancy-containing Sc_2CO_2 Monolayer

By optimization calculations, we have determined the adsorption energy, adsorption distance, and the change of bond length in gas molecules after being adsorbed on the Sc2CO2 monolayer (Table 1). The most preferred adsorption site of each gas molecule is the position where the system's total energy reaches the smallest value, which also means that the adsorption energy is maximum [21, 29]. Accordingly, the most preferred adsorption sites of H_2O, N_2, and NH_3 molecules are all located at position B (at the top of the Sc atom in the 2nd atomic layer) and close to the vacancy (Figure 2 (a, c, e)). Meanwhile, the most preferred adsorption site of H_2 and H_2S molecules is the C site (Figure 2 (b, d)). It is noteworthy that in our optimization calculations, the H_2O molecule always tends to shift to the B site from all the adsorption sites around the vacancy.

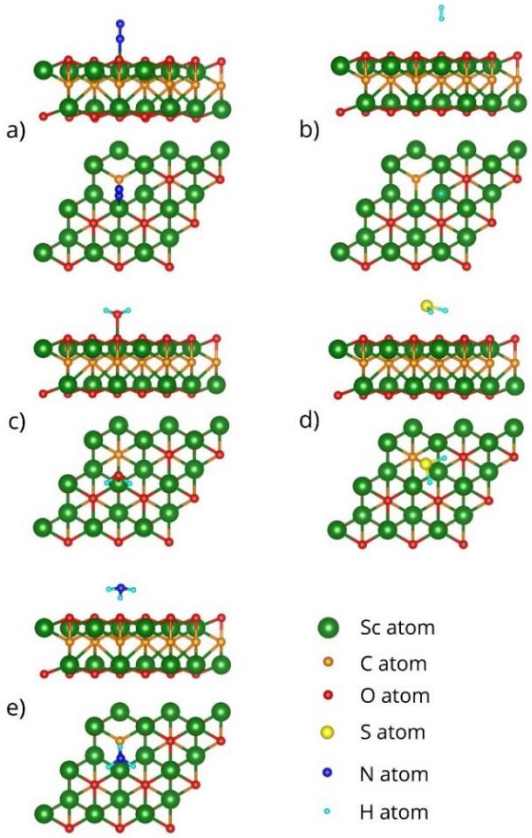

Figure 2. Side view and top view of the most favorable configurations of the O-vacancy-containing Sc_2CO_2 monolayer after adsorption of N_2 (a), H_2 (b), CO_2 (c), H_2S (d), NH_3 (e) molecules.

The H_2 molecule interacts very weakly with the O-vacancy-containing Sc_2CO_2 monolayer at all adsorption sites, with very small adsorption energy (0.03 eV), significant adsorption distance (3.250

Å) and negligible charge transfer between the monolayers layer and the H_2 molecule (0.013 e at the A site). In addition, the bond length between two H atoms is almost unchanged before and after adsorption.

At the most preferred adsorption site, N_2 molecule is inclined to the surface of the monolayer with an adsorption distance of 2.367 Å (Figure 2a). At this position, the charge transfers from the monolayer to N_2 molecule is up to 0.163 e. The bond length between two N atoms in the N_2 molecule increases by 0.8%. On the PDOS of atoms neighboring the vacancy, we can observe the hybridization between the N-*2p* orbital of the N_2 molecule with the C-*2p* orbital on the Sc_2CO_2 monolayer at an energy level of 0.4 eV (Fig. 3c).

Table 1. H_2, N_2, NH_3, H_2S and H_2O gas adsorption properties on the O-vacancy-containing Sc_2CO_2 monolayer: Eads adsorption energy, d_{ads} adsorption distance, charge transfer from the Sc_2CO_2 monolayer to molecules, bond length in gas molecules before (l_0) and after being adsorbed (l). The adsorption energy values corresponding to the most preferred adsorption site of each gas are bolded.

Configurations	E_{ads} (eV)	d_{ads} (Å)	ΔQ (|e|)	l_0 (Å)	l (Å)
H_2- $Sc_2CO_2^{Ov}$ - A site	**0.03**	3.802 (d_{Sc-H})	0.013	0.761	0.762
H_2- $Sc_2CO_2^{Ov}$ - B site	0.03	3.250 (d_{Sc-H})	0.004	0.761	0.762
H_2- $Sc_2CO_2^{Ov}$ - C site	0.03	3.807 (d_{Sc-H})	0.006	0.761	0.762
N_2- $Sc_2CO_2^{Ov}$ - A site	0.08	3.786 (d_{N-Sc})	0.017	1.109	1.109
N_2- $Sc_2CO_2^{Ov}$ - B site	0.01	3.325 (d_{N-Sc})	0.031	1.109	1.110
N_2- $Sc_2CO_2^{Ov}$ - C site	**0.34**	2.367 (d_{N-Sc})	0.163	1.109	1.118
NH_3- $Sc_2CO_2^{Ov}$ - A site	0.31	3.076 (d_{H-Sc})	0.003	1.127 1.127 1.127	1.027 1.027 1.027
NH_3- $Sc_2CO_2^{Ov}$ - B site	**0.55**	2.594 (d_{H-Sc})	0.022	1.127 1.127 1.127	1.025 1.026 1.031
NH_3- $Sc_2CO_2^{Ov}$ - C site	0.40	2.936 (d_{H-Sc})	0.067	1.127 1.127 1.127	1.025 1.027 1.027
H_2S- $Sc_2CO_2^{Ov}$ - A site	0.76	2.961 (d_{S-Sc})	0.004	1.336 1.336	1.360 1.357
H_2S - $Sc_2CO_2^{Ov}$ - B site	**0.80**	2.842 (d_{S-Sc})	0.006	1.336 1.336	1.359 1.368
H_2S - $Sc_2CO_2^{Ov}$ - C site	0.74	2.814 (d_{H-Sc})	0.005	1.336 1.336	1.361 1.363
H_2O- $Sc_2CO_2^{Ov}$ - A site	**0.63**	2.401 (d_{O-Sc})	0.004	0.979 0.979	0.983 0.984
H_2O - $Sc_2CO_2^{Ov}$ - B site	0.63	2.401 (d_{O-Sc})	0.004	0.979 0.979	0.983 0.984
H_2O - $Sc_2CO_2^{Ov}$ - C site	0.63	2.401 (d_{O-Sc})	0.004	0.979 0.979	0.983 0.984

At the preferred adsorption position (B site), NH_3 molecule is inclined to the surface of the monolayer with an adsorption distance is 2.594 Å. The adsorption energy is up to 0.55 eV; however, the charge transfer is minimal (0.022 e). The bond length between N atom and H atoms in NH_3 molecule is reduced. Analysis from PDOS of atoms neighboring the vacancy area shows a hybridization between the N-*2p* atomic orbitals with the Sc-*3d* orbitals on the Sc_2CO_2 monolayer at the energy level of -3.7 eV (Figure 3d).

The preferred H_2S molecule adsorbed on the Sc_2CO_2 monolayer is at site B with an adsorption energy of 0.80 eV. The adsorption distance is quite large at 2.842 Å, and there is almost no charge transfer between them (Table 1). The H-S bond length in H_2S molecule increases to approximately 2%. On the PDOS of atoms in the adsorption area, hybridization of H*1s*-Sc*3d* atomic orbitals and S*2p*-Sc*3d*-C*2p* orbitals of the gas molecule and the monolayer occurs at energy levels of -1.4 eV and 1.3 eV.

At the preferred adsorption site (site B), the H_2O molecule is inclined to the surface of the Sc_2CO_2 monolayer with an adsorption distance is 2.401 Å. The charge transfer is not significant. However, the adsorption energy is large (0.63 eV), and the hybridization occurs between the H1s-Sc3d atomic orbitals at energy levels of 1.8 eV and 3.0 eV (Figure 3a).

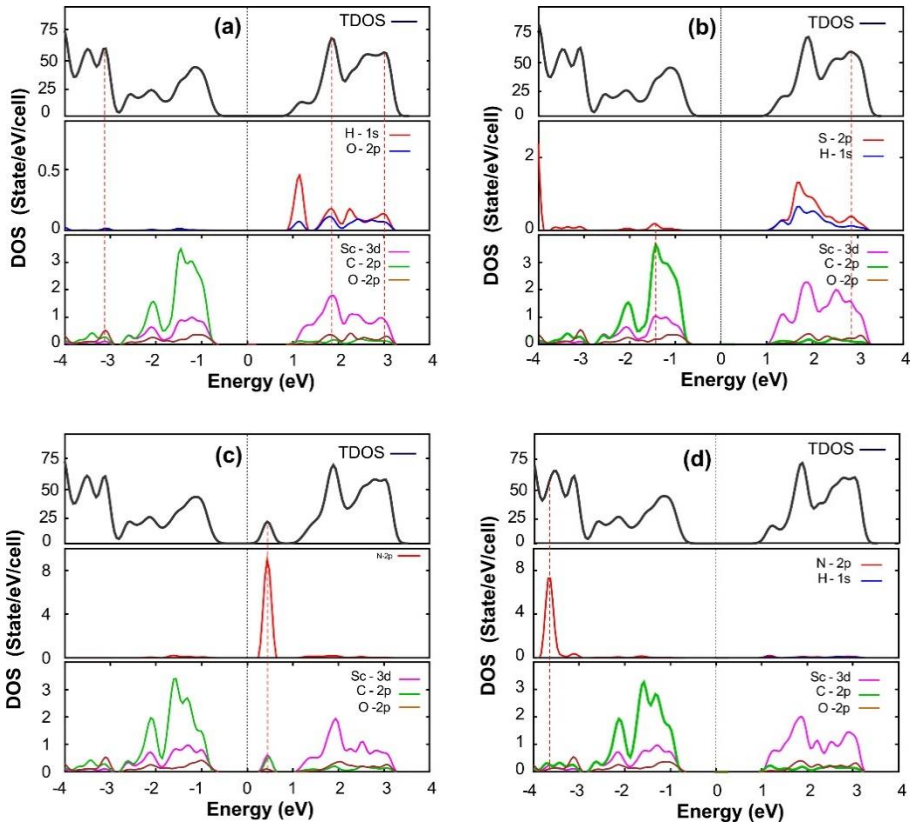

Figure 3. TDOS and DOS of the $Sc_2CO_2^{Ov}$ monolayer after adsorption of H_2O (a), H_2S (b), N_2 (c), và NH_3 (d) molecules. Hybridizations of states are shown by red dashed lines.

In general, the adsorption distances of N_2, H_2, CO_2, H_2S, and NH_3 molecules are large (from 2.367 to 3.807 Å) compared to the chemical bond length (Table 1). This is also consistent with their small adsorption energies on the Sc_2CO_2 monolayer. The gas molecules N_2, H_2, CO_2, H_2S, and NH_3 act as

acceptors, gaining electrons from the Sc_2CO_2 monolayer. However, in all adsorption of N_2, H_2, CO_2, H_2S, and NH_3 molecules, the charge transfers between the monolayer and the gas molecules are very small. The bonds between the monolayer and the N_2, H_2, CO_2, H_2S, and NH_3 gas molecules are mainly van der Wall bonds or weak covalent bonds.

3.3. Chemical Adsorption of CO_2, CO, NO_2, NO, O_2 and SO_2 Molecules at the Neighboring Area of the Oxygen Vacancy on the Sc_2CO_2 Monolayer

The calculated adsorption energy, adsorption distance, and charge transfer between CO_2, CO, NO_2, NO, O_2, and SO_2 gas molecules and Sc_2CO_2 monolayer show that their adsorption intensity is higher than that of the gas molecules described in Section 3.2.

CO_2 molecule is located perpendicular to the monolayer at the most stable adsorption position. It forms up to three O-Sc bonds and three C-Sc bonds with Sc atoms near the vacancy (Figure 4a). The O_2 adsorption energy at this position is up to 1.38 eV. CO_2 molecule acts as an acceptor with a charge transfer of the Sc_2CO_2 monolayer to the CO_2 molecule of 1.273 e. The chemical interaction between them is manifested in the hybridization of PDOS at various energy levels in the valence band and conduction band (Figure 5a). The strong interaction between the Sc_2CO_2 monolayer and the CO_2 molecule significantly increased the bond lengths in the CO_2 molecule (up to 14%) (Table 2).

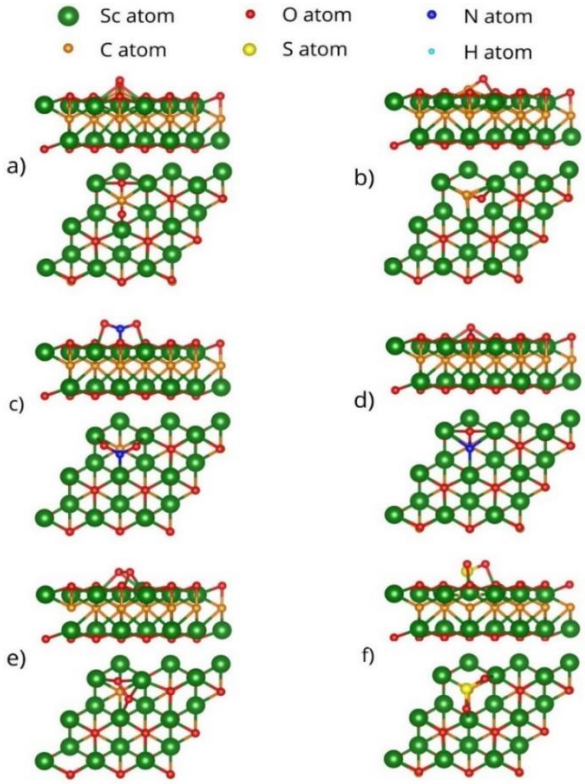

Figure 4. Side view and top view of the most favorable configurations of the O-vacancy-containing Sc_2CO_2 monolayer after adsorption of CO_2 (a), CO (b), NO_2 (c), NO (d), O_2 (e) and SO_2 (f)) molecules.

At the preferred adsorption site, CO molecule is inclined to the surface of the Sc_2CO_2 monolayer, C atom is located at the oxygen vacancy position and forms bonds with the neighboring Sc atoms and

with the C atom at the bottom with a bond distance of 1.478 Å. The charge transfer from monolayer to CO molecule is 0.989 e. On the PDOS of atoms near the vacancy area, hybridization of the C*2p* orbital with Sc*3d*, C-*2p* orbitals on the monolayer is observed (Figure 5b), which exhibits a strong chemical bond between the CO molecule and the Sc_2CO_2 monolayer.

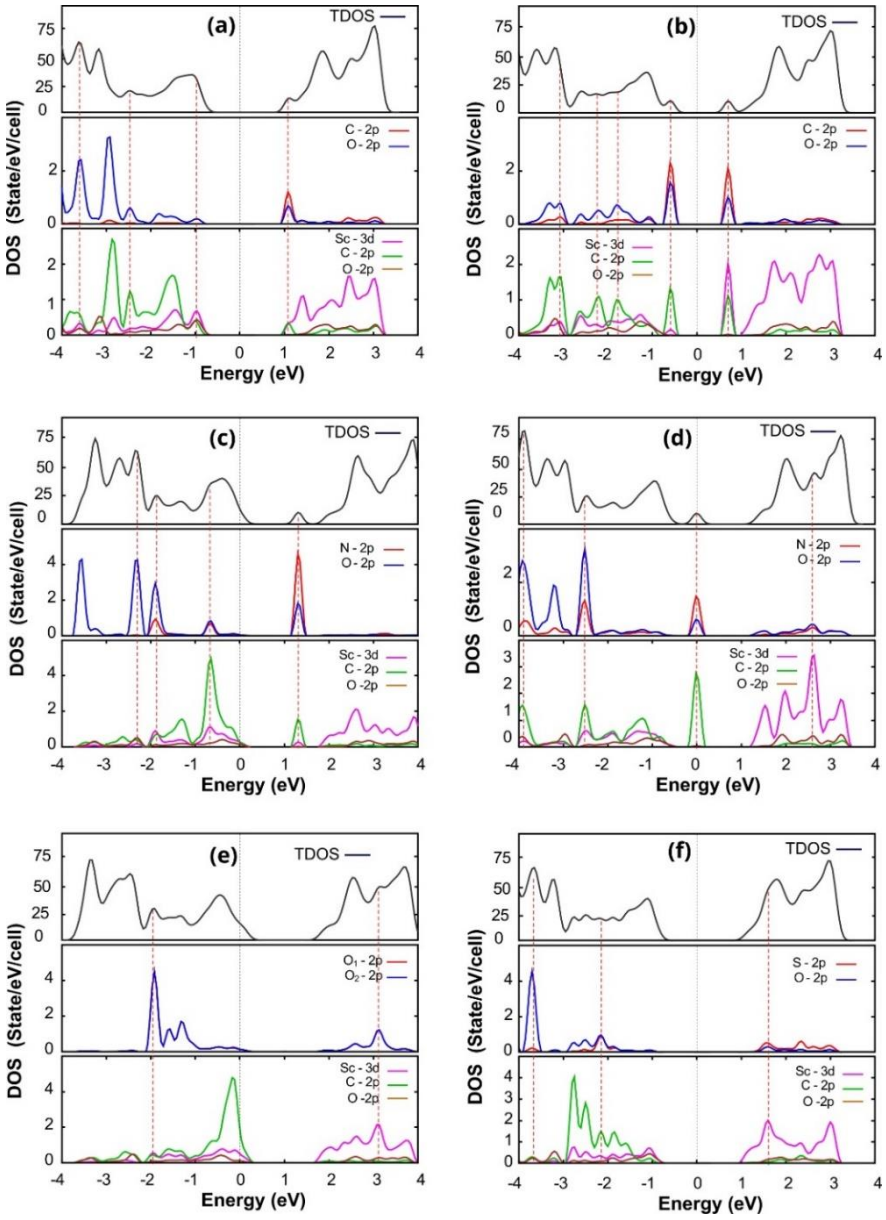

Figure 5. TDOS and DOS of $Sc_2CO_2^{Ov}$ monolayer when adsorbing CO_2 (a), CO (b), NO_2 (c), NO (d), O_2 (e), and SO_2 (f) gas molecules. Hybridizations of states are shown by red dashed lines.

The most preferred adsorption site of the NO_2 molecule adsorbed on the O-vacancy-containing Sc_2CO_2 monolayer is at the vacancy site (Figure 4c) with an adsorption energy of 2.72 eV. Each atom in the NO_2 molecule forms a bond with a Sc atom located around the oxygen vacancy. The chemical

bond between NO_2 molecule and the Sc_2CO_2 monolayer is evident in the hybridization of the Sc*3d*, N-*2p* and O-*2p* states at the energies of -2.3 eV, -1.8 eV, -0.7 eV and 1.3 eV. The NO_2 molecule acts as an acceptor with a charge transfer equal to 1.058 e.

Table 2. O_2, NO and SO_2 gas adsorption characteristics on Sc_2CO_2 monolayer: E_{ads} adsorption energy, d_{ad} adsorption distance, charge transfer from the Sc_2CO_2 monolayer to molecules Q_{tran}, bond length in gas molecules before (l_0) and after (l) adsorption

Configuration	E_{ads} (eV)	d_{ad}	Q_{tran} (|e|)	l_0 (Å)	l (Å)
CO_2-$Sc_2CO_2^{Ov}$ - A site	1.38	2.089 (d_{O-Sc})	1.273	1.172 1.172	1.336 1.289
CO_2- $Sc_2CO_2^{Ov}$ - B site	0.26	2.666 (d_{O-Sc})	0.021	1.172 1.172	1.178 1.166
CO_2- $Sc_2CO_2^{Ov}$ - C site	0.28	2.979 (d_{O-Sc})	0.039	1.172 1.172	1.178 1.167
CO- $Sc_2CO_2^{Ov}$ - A site	1.07	1.478 (d_{C-C})	0.989	1.142	1.299
CO- $Sc_2CO_2^{Ov}$ - B site	0.78	1.707 (d_{C-C})	0.972	1.142	1.289
CO- $Sc_2CO_2^{Ov}$ - C site	0.73	2.260 (d_{Sc-C})	0.499	1.142	1.188
NO- $Sc_2CO_2^{Ov}$ - A site	3.19	1.439 (d_{N-C})	2.051	1.159	1.466
NO- $Sc_2CO_2^{Ov}$ - B site	3.19	1.439 (d_{N-C})	2.051	1.159	1.466
NO- $Sc_2CO_2^{Ov}$ - C site	3.19	1.439 (d_{N-C})	2.051	1.159	1.466
SO_2- $Sc_2CO_2^{Ov}$ - A site	1.93	1.874 (d_{S-C})	0.827	1.453 1.453	1.532 1.532
SO_2- $Sc_2CO_2^{Ov}$ - B site	0.89	2.227 (d_{O-Sc})	0.469	1.453 1.453	1.525 1.478
SO_2- $Sc_2CO_2^{Ov}$ - C site	1.48	2.187 (dO-Sc)	0.692	1.453 1.453	1.522 1.522
NO_2- $Sc_2CO_2^{Ov}$ - A site	2.72	2.193 (d_{O-Sc})	1.058	1.210 1.210	1.297 1.295
NO_2- $Sc_2CO_2^{Ov}$ - B site	2.47	2.394 (d_{O-Sc})	0.871	1.210 1.210	1.354 1.217
NO_2- $Sc_2CO_2^{Ov}$ - C site	2.32	2.317 (d_{O-Sc})	0.835	1.210 1.210	1.233 1.347
O_2- $Sc_2CO_2^{Ov}$ - A site	3.64	2.111 (d_{O-O})	1.342	1.229	1.491
O_2- $Sc_2CO_2^{Ov}$ - B site	3.64	2.111 (d_{O-O})	1.339	1.229	1.491
O_2- $Sc_2CO_2^{Ov}$ - C site	2.61	2.086 (d_{O-O})	1.261	1.229	1.460

NO molecule is chemisorbed at the O-vacancy on the Sc_2CO_2 monolayer area (Figure 4d). Here is the most preferred adsorption site of NO molecules on the Sc_2CO_2 monolayer with an adsorption energy of 3.19 eV. N atom is adsorbed at the oxygen vacancy position and creates bonds to three Sc atoms and C atoms with lengths of 2.187 Å, 2.187 Å, 2.011 Å, and 1.439 Å, respectively. O atom is further bonded to two Sc atoms with a distance of 2.12 Å. The bond length in the NO molecule increased from 1.159 Å to 1.385 Å after being adsorbed at the vacancy position. On the PDOS of atoms neighboring the vacancy, hybridization between the N-*2p* orbitals with Sc-*3d* and C-*2p* can be

observed at the energies of -2.5 eV, 0 eV, and 2.6 eV (Figure 5d). The NO molecule acts as an acceptor with a charge transfer from the monolayer equal to 2.051 e.

O_2 and SO_2 molecules were also chemisorbed on the Sc_2CO_2 monolayer containing an oxygen vacancy with significant adsorption energy and a small adsorption distance (Table 2). O_2 molecule is horizontal above the vacancy site and forms four O-Sc bonds with the monolayer. In general, the formation of chemical bonding is demonstrated by the strong hybridization of the atomic orbitals of the gas molecules and the Sc_2CO_2 monolayer. In addition, the significant adsorption energy, the significant charge transfer, and the small adsorption distance (about 1.5÷2.1 Å) show that CO_2, CO, NO_2, NO, O_2 and SO_2 are chemisorbed on the O-vacancy-containing Sc_2CO_2 monolayer.

The adsorption energy for O_2 molecule is the largest compared to the other molecules (Table 2). This shows that the selectivity in gas adsorption on the Sc_2CO_2 monolayer belongs to O_2 gas. Note that the selectivity of the original Sc_2CO_2 monolayer also belongs to oxygen molecules [21]. Thus, the existence of O-vacancy does not change the oxygen adsorption selectivity of the Sc_2CO_2 monolayer. However, compared with the gas adsorption properties of the ideal Sc_2CO_2 monolayer [21], the calculated results in this study showed that the oxygen vacancy on the Sc_2CO_2 monolayer enhances the CO and CO_2 adsorption intensities compared with the original Sc_2CO_2 monolayer. The original Sc_2CO_2 monolayer physically adsorbs CO and CO_2 gas molecules with adsorption energies of 0.03 eV and 0.04 eV, respectively. Meanwhile, the optimization calculations show that the CO and CO gas molecules are chemisorbed to the O vacancy position with adsorption energies up to 1.38 eV and 1.07 eV, respectively. Thus, the existence of the O-vacancy changes the gas adsorption intensity on the Sc_2CO_2 monolayer, which is consistent with the similar results reported in Refs [32, 33].

From the calculated data in Table 1 and Table 2, we found no proportional relationship between the adsorption energy and the charge transfer for different gas molecules. For example, the adsorption energy of CO molecules is slightly greater than that of CO (1.07 eV and 0.80 eV, respectively). Still, the charge transfer from the monolayer to the CO molecule is far superior to that of H_2S (0.989 e and 0.006 e, respectively). This shows the different bonding nature between the gas molecules and the Sc_2CO_2 monolayer. The significant charge transfer to CO molecule corresponds to its ionic bond with the Sc_2CO_2 monolayer, while the small charge transfer to H_2S molecule corresponds to the van der Wall interactions.

All studied gas molecules act as acceptors upon physical adsorption or chemisorption into the O-vacancy area on the Sc_2CO_2 monolayer. Among them, the charge transfer from the O-vacancy-containing Sc_2CO_2 monolayer to NO molecule (2.051 e) is much larger than that of other molecules. Because of its electron donor properties when adsorbing NO gas with the significant charge transfer, the O-vacancy-containing Sc_2CO_2 monolayer can be applied to resistive sensors to detect NO gas.

4. Conclusion

In this work, we have systematically studied (N_2, H_2, O_2, NO, NO_2, CO, CO_2, SO_2, H_2S, H_2O, and NH_3) gases adsorption properties on the O-vacancy-containing Sc_2CO_2 monolayer based on calculations from density functional theory. The preferred adsorption sites for each gas were determined based on optimization calculations by the least principle of total energy. The calculated results showed that H_2, N_2, NH_3, H_2S, and H_2O molecules are physisorbed, while CO_2, CO, NO_2, NO, O_2, and SO_2 molecules are chemisorbed in the neighboring area of the oxygen vacancy on the Sc_2CO_2 monolayer. The oxygen vacancies on the Sc_2CO_2 monolayer significantly enhanced the CO and CO_2 adsorption intensity compared to the pristine Sc_2CO_2 monolayer. Our research results show that the O-vacancy-containing Sc_2CO_2 monolayer can be used for the fabrication of NO gas resistive sensors.

Acknowledgments

This research is funded by Vietnam National Foundation for Science and Technology Development (NAFOSTED) under grant number 103.01-2019.308.

References

[1] G. Korotcenkov, Handbook of Gas Sensor Materials, Properties, Advantages and Shortcomings for Applications, Springer, New York, 2013, https://doi.org/10.1007/978-1-4614-7165-3.

[2] X. Tang, A. Du, L. Kou, Gas Sensing and Capturing Based on Two-Dimensional Layered Materials: Overview from Theoretical Perspective, Wiley Interdisciplinary Reviews: Computational Molecular Science, Vol. 8, No. 4, 2018, https://doi.org/e1361. 10.1002/wcms.1361.

[3] M. M. Rana, D. S. Ibrahim, M. M. Asyraf, S. Jarin, A. Tomal, A Review on Recent Advances of CNTs as Gas Sensors, Sensor Review, Vol. 37, 2017, pp. 127-136, https://doi.org/10.1038/s41467-019-10297-8.

[4] H. Nazemi, A. Joseph, J. Park, A. Emadi, Advanced Micro- and Nano-Gas Sensor Technology: A Review, Sensors, Vol. 19, 2019, pp. 1285, https://doi.org/10.1108/SR-10-2016-0230.

[5] M. Naguib, M. Kurtoglu, V. Presser, J. Lu, J. Niu, M. Heon, L. Hultman, Y. Gogotsi, M. W. Barsoum, Two-Dimensional Nanocrystals Produced by Exfoliation of Ti_3AlC_2, Advanced Materials, Vol. 23, 2011, pp. 4248-4253, https://doi.org/10.1002/adma.201102306.

[6] J. Wang, T. N. Ye, Y. Gong, J. Wu, N. Miao, T. Tada, H. Hosono, Discovery of Hexagonal Ternary Phase Ti_2InB_2 and Its Evolution to Layered Boride TiB, Nature Communications, Vol. 10, 2019, pp. 1-8, https://doi.org/10.1038/s41467-019-10297-8.

[7] N. Miao, J. Wang, Y. Gong, J. Wu, H. Niu, S. Wang, K. Li, A. R. Oganov, T. Tada, H. Hosono, Computational Prediction of Boron-based MAX Phases and MXene Derivatives, Chemistry of Materials, Vol. 32, 2020, pp. 6947-6957, https://doi.org/10.1021/acs.chemmater.0c02139.

[8] M. Naguib, V. N. Mochalin, M. W. Barsoum, Y. Gogotsi, 25th Anniversary Article: MXenes: A New Family of Two-Dimensional Materials, Advanced Materials, Vol. 26, 2014, pp. 992-1005, https://doi.org/10.1002/adma.201304138.

[9] J. Zhu, E. Ha, G. Zhao, Y. Zhou, D. Huang, G. Yue, L. Hu, N. Sun, Y. Wang, L. Y. S. Lee, Recent Advance in MXenes: A promising 2D Material for Catalysis, Sensor and Chemical Adsorption, Coordination Chemistry Reviews, Vol. 352, 2017, pp. 306-327, https://doi.org/10.1016/j.ccr.2017.09.012.

[10] A. Junkaew, R. Arroyave, Enhancement of the Selectivity of MXenes (M_2C, M= Ti, V, Nb, Mo) via Oxygen-Functionalization: Promising Materials for Gas-sensing and -separation, Physical Chemistry Chemical Physics, Vol. 20, 2018, pp. 6073-6082, https://doi.org/10.1039/C7CP08622A.

[11] B. M. Jun, S. Kim, J. Heo, C. M. Park, N. Her, M. Jang, Y. Huang, J. Han, Y. Yoon, Review of MXenes as New Nanomaterials for Energy Storage/delivery and Selected Environmental Applications, Nano Research, Vol. 12, 2019, pp. 471-487, https://doi.org/10.1007/s12274-018-2225-3.

[12] X. F. Yu, Y. C. Li, J. B. Cheng, Z. B. Liu, Q. Z. Li, W. Z. Li, X. Yang, B. Xiao, Monolayer Ti_2CO_2: A Promising Candidate for NH_3 Sensor or Capturer with High Sensitivity and Selectivity, ACS Applied Materials & Interfaces, Vol. 7, 2015, pp. 13707-13713, https://doi.org/10.1021/acsami.5b03737.

[13] I. Persson, J. Halim, H. Lind, T. W. Hansen, J. B. Wagner, L. Å. Näslund, V. Darakchieva, J. Palisaitis, J. Rosen, P.O. Persson, 2D Transition Metal Carbides (MXenes) for Carbon Capture, Advanced Materials, Vol. 31, 2019, pp. 1805472, https://doi.org/10.1002/adma.201805472.

[14] A. Taheri Najafabadi, CO_2 Chemical Conversion to Useful Products: An Engineering Insight to the Latest Advances Toward Sustainability, International Journal of Energy Research, Vol. 37, 2013, pp. 485-499, https://doi.org/10.1002/er.3021.

[15] E. Lee, A. VahidMohammadi, B. C. Prorok, Y. S. Yoon, M. Beidaghi, D. J. Kim, Room Temperature Gas Sensing of Two-dimensional Titanium Carbide (MXene), ACS Applied Materials & Interfaces, Vol. 9, 2017, pp. 37184-37190, https://doi.org/10.1021/acsami.7b11055.

[16] Q. Hu, H. Wang, Q. Wu, X. Ye, A. Zhou, D. Sun, L. Wang, B. Liu, J. He, Two-dimensional Sc_2C: A Reversible and High-capacity Hydrogen Storage Material Predicted by First-principles Calculations, International Journal of Hydrogen Energy, Vol. 39, 2014, pp. 10606-10612, https://doi.org/10.1016/j.ijhydene.2014.05.037.

[17] Q. Hu, D. Sun, Q. Wu, H. Wang, L. Wang, B. Liu, A. Zhou, J. He, MXene: A New Family of Promising Hydrogen Storage Medium, The Journal of Physical Chemistry A, Vol. 117, 2013, pp. 14253-14260, https://doi.org/10.1021/jp409585v.

[18] N. P. Sian, J. C. Sin, Q. J. Ai, S. M. Lam, Two-Dimensional MXene as a Promising Material for Hydrogen Storage, 2019, https://doi.org/10.21741/9781644900253-3.

[19] D. Yang, X. Fan, D. Zhao, Y. An, Y. Hu, Z. Luo, Sc2CO2 and Mn-doped Sc2CO2 as Gas Sensor Materials to NO and CO: A first-principles study, Physica E: Low-dimensional Systems and Nanostructures, Vol. 111, 2019, pp. 84-90, https://doi.org/10.1016/j.physe.2019.02.019.

[20] S. Ma, D. Yuan, Z. Jiao, T. Wang, X. Dai, Monolayer Sc_2CO_2: A Promising Candidate as a SO_2 Gas Sensor or Capturer, The Journal of Physical Chemistry C, Vol. 121, 2017, pp. 24077-24084, https://doi.org/10.1021/acs.jpcc.7b07921.

[21] K. D. Pham, T. H. Ly, T. V. Vu, L. L. Hai, H. T. T. Nguyen, P. T. T. Le, O. Y. Khyzhun, Gas Adsorption Properties (N_2, H_2, O_2, NO, NO_2, CO, CO_2, and SO_2) on a Sc_2CO_2 Monolayer: A First-principles Study, New Journal of Chemistry, Vol. 44, 2020, pp. 18763-18769, https://doi.org/10.1039/D0NJ03545A.

[22] H. P. Komsa, J. Kotakoski, S. Kurasch, O. Lehtinen, U. Kaiser, A. V. Krasheninnikov, Two-dimensional Transition Metal Dichalcogenides under Electron Irradiation: Defect Production and Doping, Physical Review Letters, Vol. 109, 2012, pp. 035503, https://doi.org/10.1103/PhysRevLett.109.035503.

[23] K. Santosh, R. C. Longo, R. Addou, R. M. Wallace, K. Cho, Impact of Intrinsic Atomic Defects on the Electronic Structure of MoS_2 Monolayers, Nanotechnology, Vol. 25, 2014, pp. 375703, https://doi.org/10.1088/0957-4484/25/37/375703.

[24] Z. Lin, B. R. Carvalho, E. Kahn, R. Lv, R. Rao, H. Terrones, M. A. Pimenta, M. Terrones, Defect Engineering of Two-dimensional Transition Metal Dichalcogenides, 2D Materials, Vol. 3, 2016, pp. 022002, https://doi.org/10.1088/2053-1583/3/2/022002.

[25] P. Giannozzi, S. Baroni, N. Bonini, M. Calandra, R. Car, C. Cavazzoni, D. Ceresoli, G. L. Chiarotti, M. Cococcioni, I. Dabo, QUANTUM ESPRESSO: A Modular and Open-source Software Project for Quantum Simulations of Materials, Journal of Physics: Condensed Matter, Vol. 21, 2009, pp. 395502, https://doi.org/10.1088/0953-8984/21/39/395502.

[26] J. P. Perdew, K. Burke, M. Ernzerhof, Generalized Gradient Approximation Made Simple, Physical Review Letters, Vol. 77, 1996, pp. 3865-3868, https://doi.org/10.1103/PhysRevLett.77.3865.

[27] J. P. Perdew, J. Chevary, S. Vosko, K. A. Jackson, M. R. Pederson, D. Singh, C. Fiolhais, Atoms, Molecules, Solids, and Surfaces: Applications of the Generalized Gradient Approximation for Exchange and Correlation, Physical Review B, Vol. 46, 1992, pp. 6671-6687, https://doi.org/10.1103/PhysRevB.46.6671.

[28] T. Bucko, J. R. Hafner, S. Lebegue, J. G. Angyán, Improved Description of the Structure of Molecular and Layered Crystals: Ab Initio DFT Calculations with Van Der Waals Corrections, The Journal of Physical Chemistry A, Vol. 114, 2010, pp. 11814-11824, https://doi.org/10.1021/jp106469x.

[29] V. V. Ilyasov, K. D. Pham, O. M. Holodova, I. V. Ershov, Adsorption of Atomic Oxygen, Electron Structure and Elastic Moduli of TiC(0 0 1) Surface During Its Laser Reconstruction: Ab Initio Study, Applied Surface Science, Vol. 351, 2015, pp. 433-444, http://dx.doi.org/10.1016/j.apsusc.2015.05.146.

[30] W. Tang, E. Sanville, G. Henkelman, A grid-based Bader Analysis Algorithm without Lattice Bias, Journal of Physics: Condensed Matter, Vol. 21, 2009, pp. 084204, https://doi.org/10.1088/0953-8984/21/8/084204.

[31] M. Yu, D. R. Trinkle, Accurate and Efficient Algorithm for Bader Charge Integration, The Journal of Chemical Physics, Vol. 134, 2011, pp. 064111, https://doi.org/10.1063/1.3553716.

[32] T. Hussain, T. Kaewmaraya, S. Chakraborty, R. Ahuja, Defect and Substitution-induced Silicene Sensor to Probe Toxic Gases, The Journal of Physical Chemistry C, Vol. 120, 2016, pp. 25256-25262, https://doi.org/10.1021/acs.jpcc.6b08973.

[33] V. V. Ilyasov, K. D. Pham, I. V. Ershov, C. V. Nguyen, N. N. Hieu, Effect of Oxygen Adsorption on Structural and Electronic Properties of Defective Surfaces (0 0 1), (1 1 1), and (1 1 0) TiC: Ab Initio Study, Computational Materials Science, Vol. 124, 2016, pp. 344-352, http://dx.doi.org/10.1016/j.commatsci.2016.08.013.